IL NUOVO CIMENTO Vol. 32 C, N. 1 Gennaio-Febbraio 2009
DOI 10.1393/ncc/i2009-10348-1

Colloquia: GCM8

A numerical homogenisation strategy for micromorphic continua

R. Jänicke and S. Diebels
Saarland University, Chair of Applied Mechanics - D-66123 Saarbrücken, Germany

(ricevuto il 3 Aprile 2009; pubblicato online il 25 Giugno 2009)

Summary. — Cellular materials are of special interest according to their peculiar mechanical properties. In this paper, special attention is paid to the simulation of size-dependent microtopological effects. We introduce a numerical homogenisation scheme for a two-scale problem dealing with a micromorphic continuum theory on the macroscale and a classical Cauchy continuum on the microscale. The transitions between both scales are obtained by projection and homogenisation rules derived from an equivalence criterion for the strain energy, also known as the Hill-Mandel condition.

PACS 46.05.+b – General theory of continuum mechanics of solids.
PACS 46.15.-x – Computational methods in continuum mechanics.

1. – Introduction and motivation

Cellular materials such as biological tissues, polymer or metal foams feature a complex mechanical behaviour. Modelling aspects to be considered are pronounced size effects resulting in boundary layers under shear, tension or bending as well as an evolving porosity and anisotropy, cf. [1-4]. For the mechanical modelling of such materials there are mainly three different approaches. The first one is to fully resolve the microstructure by beam or continuum elements within the finite element method (FEM). This approach is on the one hand able to capture the microtopological effects, but on the other hand one has to solve a problem with a huge amount of degrees of freedom which is, for sufficient large samples, numerically very expensive. The second approach is a purely macroscopic one, introducing extended continuum theories with additional degrees of freedom. Extended continuum formulations are treated in a general framework in [5-11]. Except for a few approaches, cf. [7], the micromotion is considered to be affine, *i.e.* it can be described by a linear mapping. The disadvantage of this second method is the necessity of additional material parameters. Those are hard to interpret from the physical point of view and, in general, hard to identify by experiments.

The third possibility is a mixed approach with the methods of the two-level FEM or FE^2 where the constitutive equations on the macroscale are replaced by a microscale calculation, cf. [12-17]. The underlying principle is the concept of scale separation, also

known as MMM principle, cf. [18], which distinguishes three different scales, the macro-, the meso- and the microscale. The macroscale covers the sample in its whole entireness whereas the mesoscale represents the microtopology, *i.e.* the cellular network. If we zoom in a microstructural element we reach the microscale which could be the atomistic scale. This second step between meso- and microscale is in general assumed to be large. Hence, we can apply continuum theories on the mesoscale. By contrast, the scale separation between the macro- and the mesoscale cannot be guaranteed in general because size-dependent microtopological effects occur, if the characteristic length scale of the mesolevel becomes comparable to that one of the macroscale. Due to the assumption the cellular network to be much larger than the atomistic level, in the following, we will use the term microscale for this microstructural scale.

In the present paper we make use of a micromorphic continuum theory allowing for finite deformations on the macroscale. To capture microtopological effects we attach a finite microvolume on every macroscopic material point. The deformation gradient and microdeformations calculated on the macroscale are projected on the microscale and define a microscopic Dirichlet boundary value problem for the attached microstructure. The analysed microvolume has to be small enough to allow for an efficient calculation and it has to be large enough to capture the characteristic features of the microtopology. For convenience we call the microvolume RVE (representative volume element). The microstructure itself is represented by a classical Cauchy continuum theory only defining displacement degrees of freedom. Hence, no extended constitutive equation has to be considered to solve the micro problem. The stress and hyper stress response of the microvolume have to be homogenised and transferred back to the macroscale by appropriate averaging procedures.

In the following sections we will formulate the fundamentals of the micromorphic continuum theory according to [8] with regard to the kinematics and to the balance laws. Analysing an energy criterion, *i.e.* an extended version of the Hill-Mandel condition, we will define projection and averaging rules. Finally, we will conclude with a numerical study and a discussion of the results.

2. – Kinematics

2˙1. *Motion and micromotion.* – Let us introduce the micromorphic continuum theory following [8] first. The physical body $\mathcal{B}$ consists of an infinitesimal set of material points P. In contrast to classical continuum theories such as the Cauchy continuum theory, every material point captures a small but finite space. The picture of each material point can be described via the position vector $\mathbf{X}$ of its centroid and an attached vector $\boldsymbol{\Xi}$ where capital letters refer to the reference configuration. An arbitrary deformation carries the system from the reference to the spatial frame. The appropriate mappings are expressed as

$$\mathbf{x} = \hat{\mathbf{x}}(\mathbf{X}, t), \tag{1a}$$

$$\boldsymbol{\xi} = \hat{\boldsymbol{\xi}}(\mathbf{X}, \boldsymbol{\Xi}, t). \tag{1b}$$

Equation (1a) leads to the definition of the deformation gradient

$$\mathrm{d}\mathbf{x} = \mathbf{F} \cdot \mathrm{d}\mathbf{X}, \tag{2a}$$

whereas eq. (1b) completes the set of motions of the micromorphic continuum of grade one if it is defined as an affine projection

$$\boldsymbol{\xi} = \bar{\boldsymbol{\chi}}(\mathbf{X},\, t) \cdot \boldsymbol{\Xi}. \tag{3a}$$

Both, eqs. (2a) and (3a), possess continuous derivatives with respect to $\mathbf{X}$ and t as well as they are invertible uniquely. The micromotion $\bar{\boldsymbol{\chi}}$ can be decomposed multiplicatively in the product of a proper orthogonal and a symmetric positive definite tensor

$$\bar{\boldsymbol{\chi}} = \bar{\mathbf{R}} \cdot \bar{\mathbf{U}}, \tag{4a}$$

where

$$\bar{\mathbf{R}}^{-1} = \bar{\mathbf{R}}^{T}, \qquad \det \bar{\mathbf{R}} = +1, \qquad \bar{\mathbf{U}} = \bar{\mathbf{U}}^{T}, \tag{5a}$$

called the microrotation tensor $\bar{\mathbf{R}}$ and the microstretch tensor $\bar{\mathbf{U}}$, respectively. The micromotion $\bar{\boldsymbol{\chi}}$ can undergo some restrictions defining a hierarchy of extended continua. If the microstretch tensor equals the second-order identity tensor $\bar{\mathbf{U}} \equiv \mathbf{I}$ the micromotion describes a pure microrotation $\bar{\boldsymbol{\chi}} = \bar{\mathbf{R}}$. This is the case for the micropolar or Cosserat continuum, named in honour of the seminal work of the brothers Cosserat in 1909 [6]. If the microstretch tensor is isotropic, $\bar{\mathbf{U}} = \bar{\jmath}\,\mathbf{I}$ where $\bar{\jmath}$ is the scalar volumetric microstretch, the microcontinuum is called microstretch continuum.

2˙2. *Deformation measures.* – We now introduce a set of three independent deformation measures,

$$\bar{\mathbf{F}} = \bar{\boldsymbol{\chi}}^{-1} \cdot \mathbf{F}, \tag{6a}$$

$$\bar{\mathbf{C}} = \bar{\boldsymbol{\chi}}^{T} \cdot \bar{\boldsymbol{\chi}} = \bar{\mathbf{U}}^{T} \cdot \bar{\mathbf{U}} \quad \text{and} \tag{6b}$$

$$\bar{\boldsymbol{\Gamma}} = \bar{\boldsymbol{\chi}}^{-1} \cdot \operatorname{Grad} \bar{\boldsymbol{\chi}}, \tag{6c}$$

where $\bar{\mathbf{F}}$ is denoted as the microdeformation tensor, $\bar{\mathbf{C}}$ as the right Cauchy-Green microdeformation tensor and $\bar{\boldsymbol{\Gamma}}$ as the wryness or curvature tensor, respectively. Capital differential operators are calculated w. r. t. the reference configuration, *i.e.* $\operatorname{Grad}(\diamond) = \partial(\diamond)/\partial\mathbf{X}$. This set of deformation measures is form invariant and it uniquely determines the motion and the micromotion, cf. [8]. Pay attention to the fact that the micropolar continuum captures an outstanding position within the micromorphic continua because eq. (6b) is reduced to the identity

$$\bar{\mathbf{C}} \equiv \mathbf{I} \tag{7a}$$

in that special case. Hence, the micropolar continuum can be described by a set of only two deformation measures. Further on we want to remark that, in contrast to the two-field character of the macroscopic deformation gradient $\mathbf{F}$, all depicted deformation measures are completely defined on the reference configuration.

3. – Balance laws

In the following section the balance equations for the micromorphic continuum are formulated in a total Lagrangian regime, *i.e.* with respect to the reference configuration, and for the static case. For elastic material behaviour they can be derived, *e.g.*, via a potential approach within the Hamilton formalism, cf. [8].

The balance of momentum reads

$$\operatorname{Div}\mathbf{P} + \rho_0\,\mathbf{b} = \mathbf{0} \tag{8a}$$

with the first Piola-Kirchhoff stress tensor $\mathbf{P}$ and the volume force $\rho_0\,\mathbf{b}$. The second balance law we take into account is the balance of moment of momentum. In contrast to the Cauchy continuum, where this balance law justifies the symmetry of the Cauchy stress tensor $\mathbf{T}$, the higher-order theory requires a coupling between stresses and hyper stresses. In the micropolar case, the hyper stress can easily be interpreted as the couple stress and the balance law reduces to the well-known balance of angular momentum

$$\operatorname{Div}\mathbf{M} + \mathbf{F}\times\mathbf{P} = \mathbf{0}. \tag{9a}$$

The physical interpretation of the micromorphic hyper stress is not so obvious because in classical engineering we are not used in dealing with, *e.g.*, axial moments. The balance of moment of momentum reads

$$\operatorname{Div}\mathbf{Q} + (\mathbf{P}-\mathbf{S})\cdot\mathbf{F}^{T} + \rho_0\,\mathbf{c} = \mathbf{0}, \tag{10a}$$

where $\mathbf{Q}$ describes the third-order couple stress of the first Piola-Kirchhoff type and $\mathbf{S}\cdot\mathbf{F}^{T}$ a further symmetric hyper stress tensor of grade two, cf. [8]. $\mathbf{S}$ again is of the first Piola-Kirchhoff type, $\rho_0\,\mathbf{c}$ describes volume couples. The transformations between stress quantities of the first Piola-Kirchhoff type and stress quantities of the Cauchy type are given as

$$\mathbf{P} = (\det\mathbf{F})\,\mathbf{T}\cdot\mathbf{F}^{T-1}, \tag{11a}$$

$$\mathbf{Q} = (\det\mathbf{F})\,\breve{\mathbf{Q}}\cdot\mathbf{F}^{T-1} \quad \text{and} \tag{11b}$$

$$\mathbf{S} = (\det\mathbf{F})\,\breve{\mathbf{S}}\cdot\mathbf{F}^{T-1}, \tag{11c}$$

where the Cauchy couple and hyper stresses are denoted by $\breve{\circ}$. The third balance law we want to focus on is the balance of internal energy which can be written as

$$\rho_0\,\varepsilon' = \bar{\mathbf{P}} : \bar{\mathbf{F}}' + \bar{\mathbf{S}} : \bar{\mathbf{C}}' + \bar{\mathbf{Q}} \vdots \bar{\boldsymbol{\Gamma}}', \tag{12a}$$

where primed quantities denote the material time rate. According to the fact all deformation quantities eqs. (6*a*)–(6*c*) to be completely defined w. r. t. the reference configuration we have to transform the first Piola-Kirchhoff type stresses and hyper stresses which are

two-field quantities by definition. Therefore we introduce

$$\bar{\mathbf{P}} = \bar{\boldsymbol{\chi}}^{T} \cdot \mathbf{P}, \tag{13a}$$

$$\bar{\mathbf{S}} = \frac{1}{2}\, \bar{\boldsymbol{\chi}}^{-1} \cdot \mathbf{S} \cdot \bar{\boldsymbol{\chi}}^{T-1} \quad \text{and} \tag{13b}$$

$$\bar{\mathbf{Q}} = \bar{\boldsymbol{\chi}}^{T} \cdot \left(\mathbf{Q}^{\overset{23}{T}} \cdot \bar{\boldsymbol{\chi}}^{T-1} \right)^{\overset{23}{T}}, \tag{13c}$$

where $(\diamond)^{\overset{23}{T}}$ transposes the second and the third base system of the third-order argument.

4. – Homogenisation procedure

4˙1. *A linear-elastic constitutive law for micromorphic continua.* – To motivate the efforts to generate a numerical homogenisation procedure we first give an explicit expression of the free-energy function for micromorphic continua in a linear-elastic regime. For the free energy we take a homogeneous, quadratic function of the deformation quantities

$$\begin{aligned} \rho\, \Psi \;=\; & \mathbf{a}^{\underline{4}} :: (\bar{\mathbf{F}} \otimes \bar{\mathbf{F}}) + \mathbf{b}^{\underline{4}} :: (\mathbf{C} \otimes \mathbf{C}) + \mathbf{c}^{\underline{6}} \vdots\vdots (\bar{\boldsymbol{\Gamma}} \otimes \bar{\boldsymbol{\Gamma}}) \\ & + \mathbf{d}^{\underline{4}} :: (\bar{\mathbf{C}} \otimes \bar{\mathbf{F}}) + \mathbf{e}^{\underline{5}} \vdots : (\bar{\mathbf{C}} \otimes \bar{\boldsymbol{\Gamma}}) + \mathbf{f}^{\underline{5}} \vdots : (\bar{\boldsymbol{\Gamma}} \otimes \bar{\mathbf{F}}). \end{aligned} \tag{14a}$$

The derivations of the free energy with respect to the deformation quantities give

$$\bar{\mathbf{P}} = \frac{\partial \Psi}{\partial \bar{\mathbf{F}}}\,, \qquad \bar{\mathbf{Q}} = \frac{\partial \Psi}{\partial \bar{\boldsymbol{\Gamma}}} \qquad \text{and} \qquad \bar{\mathbf{S}} = \frac{\partial \Psi}{\partial \bar{\mathbf{S}}}\,. \tag{15a}$$

Following [19] we can reduce the number of independent material parameters in the coefficient tensors assuming an isotropic material. For the 3D case we still have to identify 18 parameters, *e.g.*, by experiments. Hence, to circumvent *a priori* the complex constitutive laws on the macroscale, we apply a two-level FEM approach. For this FE^2 calculation we assume a finite microvolume to be attached on every macroscopic material point [12-14, 17]. The microvolume contains the information of the microtopolgy on a discrete level, *i.e.* in our case the discrete cellular microstructure which we describe by a standard continuum theory. However we suppose the macroscale to be homogeneous and at the same time able to reflect higher-order effects such as boundary layer effects caused by the microtopology. Hence, we choose a micromorphic continuum theory on the macroscale as discussed before.

4˙2. *Hill-Mandel condition.* – The fundamental assumption for the subsequent homogenisation procedure is the equivalence of the strain energy in every macroscopic material point on the one hand and the volume average of the microscopic strain energy of the attached microvolume on the other hand. This correlation is commonly called Hill-Mandel condition [15, 16, 20, 21, 17, 18] and can be expressed as

$$\langle \mathbf{P}_m : \mathbf{F}_m \rangle = \bar{\mathbf{P}}_M : \bar{\mathbf{F}}_M + \bar{\mathbf{S}}_M : \bar{\mathbf{E}}_M + \bar{\mathbf{Q}}_M \vdots \bar{\boldsymbol{\Gamma}}_M. \tag{16a}$$

The volume average is depicted by $\langle \diamond \rangle$, small indices m refer to the microscale, capital indices M to the macroscale. The r. h. s. of eq. (16a) takes into account that strain

energy can be stored in an extended continuum formulation by different deformation mechanisms defined by the different deformation measures. To ensure no energy to be stored in the undeformed system we introduce the Green-Lagrange–type strain tensor

$$\bar{\mathbf{E}}_M = \bar{\mathbf{C}}_M - \mathbf{I}. \tag{17a}$$

4˙3. *Projection*. – To simplify matters we define a rectangular microvolume $\mathcal{R}_V$ with width a_1 and height a_2 in 2D where the microcoordinates X_{mi} are within the ranges

$$X_{mi} \in \left[-\frac{a_i}{2}, \frac{a_i}{2}\right]. \tag{18a}$$

We assume the displacement of an arbitrary point on the boundary of the microvolume to be calculated via a Taylor series expansion of the linear mapping similar to [15-17],

$$\mathbf{x}_m = \mathbf{F}_M \cdot \mathbf{X}_m + \frac{1}{2}\,\bar{\boldsymbol{\Gamma}}_M : (\mathbf{X}_m \otimes \mathbf{X}_m) + \frac{1}{6}\,\overset{4}{\bar{\mathbf{E}}}_M \,\vdots\, (\mathbf{X}_m \otimes \mathbf{X}_m \otimes \mathbf{X}_m) + \tilde{\mathbf{x}}_m, \tag{19a}$$

where $\tilde{\mathbf{x}}_m$ represents a fluctuation field due to the microstructural periodicity. The fourth-order hyper strain tensor $\overset{4}{\bar{\mathbf{E}}}_M$ can be reduced to the second-order Green-Lagrange microstrain tensor $\bar{\mathbf{E}}_M$. We choose

$$\mathbf{M} \cdot \bar{\mathbf{E}}_M \cdot \mathbf{M}^T = \overset{4}{\mathbf{D}} \,\vdots\, \overset{4}{\bar{\mathbf{E}}}_M, \tag{20a}$$

where for dimensional reasons with a Cartesian metric

$$M_{ij} \mathrel{\hat{=}} \begin{bmatrix} 1/a_1 & 0 \\ 0 & 1/a_2 \end{bmatrix} \tag{21a}$$

and

$$\overset{4}{\mathbf{D}} = \delta_{ijkl}\mathbf{e}_i \otimes \mathbf{e}_j \otimes \mathbf{e}_k \otimes \mathbf{e}_l, \tag{22a}$$

$$\delta_{ijkl} = \begin{cases} 1, & \text{all indices equal the same value,} \\ -1, & \text{indices are pairwise equal,} \\ 0, & \text{otherwise.} \end{cases} \tag{22b}$$

It can be shown that the cubic part of the polynomial (19a) is complete but, due to the restriction to the second-order Green-Lagrange microstrain tensor $\bar{\mathbf{E}}_M$, the cubic polynomial links are not initiated independently from each other, cf. for the 2D case with a Cartesian metric

$$x_{mi}^{\text{cubic}} \mathrel{\hat{=}} \frac{1}{6} \begin{bmatrix} \frac{1}{4\,a_1^2}\,\bar{E}_{M11} X_{m1}^3 + \frac{3}{4\,a_1 a_2}\,\bar{E}_{M12} X_{m1}^2\, X_{m2} \\ -\frac{1}{4\,a_1 a_2}\,\bar{E}_{M12}\, X_{m1}^3 - \frac{3}{4\,a_2^2}\,\bar{E}_{M22}\, X_{m1}^2\, X_{m2} \\ -\frac{3}{4\,a_1^2}\,\bar{E}_{M11}\, X_{m1}\, X_{m2}^2 - \frac{1}{4\,a_1 a_2}\,\bar{E}_{M12}\, X_{m2}^3 \\ +\frac{3}{4\,a_1 a_2}\,\bar{E}_{M12}\, X_{m1}\, X_{m2}^2 + \frac{1}{4\,a_2^2}\,\bar{E}_{M22}\, X_{m2}^3 \end{bmatrix}. \tag{23a}$$

In the most general case of the micromorphic continuum the quadratic polynomial is complete and the quadratic links are uncorrelated. With the restriction to the microstretch continuum the cubic polynomial is not longer complete, cf. eq. (23a) with $\bar{E}_{M11} = \bar{E}_{M22}$ and $\bar{E}_{M12} = 0$, whereas the quadratic polynomial is complete but its links are correlated cf. in 2D

$$x_{mi}^{\text{quadratic}} \mathrel{\hat{=}} \frac{1}{2} \begin{bmatrix} \overset{*}{\bar{\boldsymbol{\Gamma}}}_{M1}\ X_{m1}^2 + \left(\overset{*}{\bar{\boldsymbol{\Gamma}}}_{M2} - \bar{\boldsymbol{\kappa}}_{M31} \right) X_{m1}\, X_{m2} - \bar{\boldsymbol{\kappa}}_{M32}\, X_{m2}^2 \\ \bar{\boldsymbol{\kappa}}_{M31}\, X_{m1}^2 + \left(\overset{*}{\bar{\boldsymbol{\Gamma}}}_{M1} + \bar{\boldsymbol{\kappa}}_{M32} \right) X_{m1}\, X_{m2} + \overset{*}{\bar{\boldsymbol{\Gamma}}}_{M2}\ X_{m2}^2 \end{bmatrix} \tag{24a}$$

with

$$\overset{*}{\bar{\boldsymbol{\Gamma}}} = \frac{1}{\bar{j}} \operatorname{Grad} \bar{j}, \tag{25a}$$

$$\bar{\boldsymbol{\kappa}} = -\frac{1}{2}\ \overset{3}{\mathbf{E}} : (\bar{\mathbf{R}}^T \cdot \operatorname{Grad} \bar{\mathbf{R}}). \tag{25b}$$

$\overset{3}{\mathbf{E}}$ is the third-order permutation tensor. In the case of the micropolar continuum there is no cubic link and the quadratic part of the polynomial is neither complete nor uncorrelated, cf. eq. (24a), (25a) with $\bar{j} = 1$.

4˙4. *Averaging theorems.* – Inserting eq. (19a) in eq. (16a) leads to the averaging theorems

$$\bar{\mathbf{F}}_M = \langle \mathbf{F}_m \rangle \tag{26a}$$

and

$$\bar{\mathbf{P}}_M = \frac{1}{V_{\mathcal{R}}} \int\limits_{\partial \mathcal{B}_{\mathcal{R}}} (\mathbf{p}_m \otimes \mathbf{X}_m)\, \mathrm{d}A, \tag{27a}$$

$$\bar{\mathbf{Q}}_M = \frac{1}{2\, V_{\mathcal{R}}} \int\limits_{\partial \mathcal{R}} (\mathbf{p}_m \otimes \mathbf{X}_m \otimes \mathbf{X}_m)\, \mathrm{d}A \qquad \text{and} \tag{27b}$$

$$\overset{4}{\bar{\mathbf{S}}}_M = \frac{1}{6\, V_{\mathcal{R}}} \int\limits_{\partial \mathcal{B}\mathcal{R}} (\mathbf{p}_m \otimes \mathbf{X}_m \otimes \mathbf{X}_m \otimes \mathbf{X}_m)\, \mathrm{d}A, \tag{27c}$$

cf. appendix A. Equation (26a) implies a further restriction to the cubic polynomial link in eq. (19a) whereas the quadratic link fulfils the same identity automatically.

The microscopic stress vector $\mathbf{p}_m$ is connected to the first Piola-Kirchhoff stress tensor and the outer normal vector via the Cauchy theorem $\mathbf{p}_m = \mathbf{P}_m \cdot \mathbf{N}$. The present calculation of the effective stresses and hyper stresses via a surface integration can be transformed to a volume averaging method proposed, *e.g.*, in [15, 16]. However in our opinion a surface formulation dealing with reaction forces on the boundary of the microvolume seems to be more convenient from the physical point of view. Moreover we

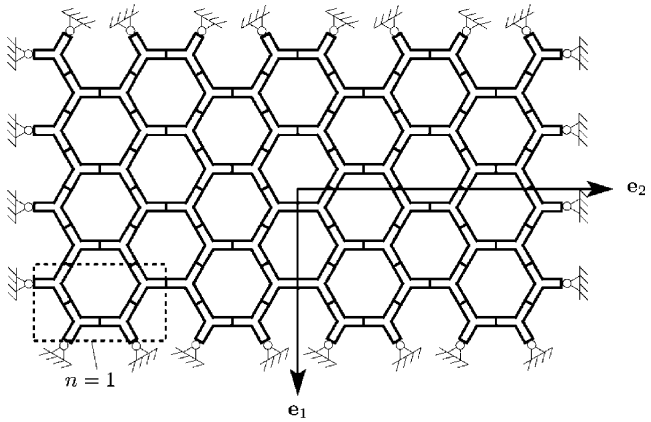

Fig. 1. – Pin-pointed cellular microstructure of the size $n = 4$ and unit cell $n = 1$.

assume the same symmetry condition, cf. $(20a)$, to be valid for the fourth-order hyper stress tensor $\overset{4}{\bar{\mathbf{S}}}_M$ as well,

$$\mathbf{M}^{-1} \cdot \bar{\mathbf{S}} \cdot \mathbf{M}^{T-1} = \overset{4}{\mathbf{D}} \vdots \overset{4}{\bar{\mathbf{S}}} . \tag{28a}$$

This assumption is due to the fact that the nonsymmetric part of the hyper stress does not produce any energy following $(16a)$. In fact, this restriction does not hold for any arbitrarily chosen heterogeneous microstructure. If so, the micromorphic continuum is not sufficient to describe the microtopological effects.

5. – Numerical studies: The microvolume size

In this section the influence of the size of the microvolume is investigated for the different types of deformation modes (linear, quadratic, cubic). We choose a regular 2D honeycomb microstructure, cf. fig. 1. The structure itself is discretised by 8-node quadrilateral continuum elements. The microscale material is assumed to be hyperelastic and follows a compressible Neo-Hooke–type material law

$$\mathbf{T}_m = \lambda_m \left[(J-1) + \frac{1}{J} \ln(J) \right] \mathbf{I} + \mu_m \left(\mathbf{F}_m \cdot \mathbf{F}_m^T - \mathbf{I} \right) . \tag{29a}$$

The microscopic material parameters $\mu_m = 1.7\,\mathrm{MPa}$ and $\lambda_m = 1\,\mathrm{MPa}$ are artificially chosen. The microscopic Dirichlet boundary conditions are defined following eq. $(19a)$. Prescribing the displacement in every point of the boundary leads to the Voigt case, the upper bound stiffness of the system. This is in fact comparable to a situation where the beam-like elements are clamped at the boundary. If we relax the system we can expect more convenient results. For the following analysis we pin-point every structural element on the boundary. Pin-pointed discrete microstructures are known to undergo a soft boundary layer effect. But this effect converges much better with increasing size of the microvolume than the stiff effect caused by clamping the beam-like elements. Hence, no periodic boundary conditions are taken into account. The influence of the boundary

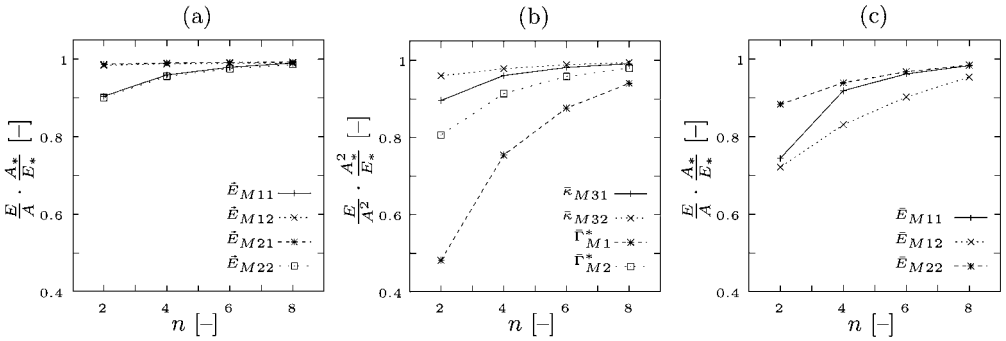

Fig. 2. – Convergence of the strain energy with increasing microvolume size for (a) linear, (b) quadratic and (c) cubic modes. The strain energy is normalised with respect to the strain energy of a large microvolume.

conditions on the stiffness of the microvolume is investigated, *e.g.*, in [22]. All convergence studies in the following are examined within the regime of small deformations. The depicted strain energies E over the microvolume A are normalised with respect to the strain energy E_* of a large microvolume A_* which is considered to be completely converged.

In fig. 2 (a) the normalised strain energy per area (which represents the microvolume in 2D) caused by the depicted linear deformation modes is plotted over the size of the microvolume. The error due to the pin-pointed situation at the boundary decreases with an increasing microvolume size. We can observe that this decay is very fast for the shear modes depending on $\tilde{E}_{M12}$ and $\tilde{E}_{M21}$. Already for a microvolume size of two times two unit cells there is nearly no measurable error in the normalised energy due to the boundary conditions. In contrast to this about six unit cells in each direction are necessary for the convergence of the stretch modes depending on $\tilde{E}_{M11}$ and $\tilde{E}_{M22}$.

In fig. 2 (b) the quadratic modes of a microstretch continuum are investigated. The normalised strain energy converges with $[1/A^2]$. This is in analogy to the moment of inertia of beams. And, in fact, this is exactly the point where the transition of the macroscopic and the microscopic length scales comes into play. A very large microstructure stores a lot more of volume-averaged strain energy as, according to bending effects, a small one does. In consequence the stimulation of the particular quadratic modes is in this case not convenient from the energetic point of view. Hence, balancing the system, the curvature tensor will be adequately small. In the limiting case of an infinitely large microvolume the solution coincides with the curvature free Cauchy solution. If, in contrast, the microvolume is chosen small the sizes of the microscopic and the macroscopic length scales become comparable. This is the precondition for size-depending higher-order effects such as boundary layer effects and it justifies the application of extended continuum theories on the macroscale.

What is noticeable is the much bigger error due to the soft boundary layer compared to the linear modes. Especially for the pure microstretch modes depending on $\overset{*}{\bar{\Gamma}}_{M1}$ and $\overset{*}{\bar{\Gamma}}_{M2}$ with a microvolume of eight times eight unit cells this error still ranges at about six percent.

In fig. 2 (c), for the cubic deformation modes of a fully micromorphic continuum, the normalised strain energy is observed to converge again over the area of the microstructure,

over the microvolume, respectively. This relation is backing up the connection between cubic and linear modes. Therefore one may acknowledge that, even if the cubic modes should certainly be called higher modes, the volume average of their strain energy depends not on the size of the microvolume. Hence, in this case, no length information is transported between the macro- and the microscale.

Concerning the soft boundary layer effect we find a faster decay for the cubic microstretch modes depending on $\bar{E}_{M11}$ and $\bar{E}_{M22}$ than for the microshear mode depending on $\bar{E}_{M12}$. For a microvolume of eight unit cells in each direction the worst error adds up to about five percent.

6. – Discussion and conclusions

In the previous sections we have worked out a numerical homogenisation procedure dealing with an extended continuum (micropolar, microstretch, micromorphic) on the macroscale and a Cauchy continuum on the microscale. On the basis of a set of three independent micromorphic deformation quantities, completely defined on the reference configuration, we have introduced the balances of moment, of moment of momentum and of internal energy. Furthermore we have derived the Hill-Mandel condition which ensures the equivalence of the stored macroscopic and volume-averaged microscopic strain energy. In the following we have defined a projection rule assigning the introduced deformation measures to the different orders of a cubic polynomial. Applying this assumption to the Hill-Mandel condition has allowed to define averaging theorems for the stresses and hyper stresses dedicated to the three deformation measures.

In the last section we have studied the dependence of the polynomial orders on the microvolume size. We have pointed out the necessity to distinguish between linear and cubic deformation modes on the one hand and quadratic deformation modes on the other hand. Whereas linear and cubic modes are not size dependent in their volume average of the strain energy, the quadratic modes are. From the physical point of view, the concept of scale separation does not hold in a consequent way because it does not allow for effects depending on the microstructural length scale.

Finally the particular decay of a soft boundary layer effect has been investigated for the different orders of deformation modes. The results show the convergence behaviour to depend strongly on the microvolume size and that the microvolume must be sufficiently large. At the same time a sufficiently large number of structural elements has to be available at the boundary to display the higher-order polynomial in a convenient way. But otherwise, other methods of relaxing the full Dirichlet boundary conditions, *e.g.*, periodic boundary conditions, also show a certain size dependence, cf. [22]. Against this background the choice of pin-pointed boundary conditions seems to be an appropriate and frugal relaxing method for cellular structures, because they necessitate neither regular meshes nor any kind of coupling relations between opposite boundaries.

Appendix A.

Proof of the homogenisation rules

Inserting eq. (19a) in eq. (16a) we calculate

$$\langle \mathbf{P}_m : \mathbf{F}_m \rangle = \frac{1}{V} \int\limits_{\partial \mathcal{B}_0} \mathbf{p}_m \cdot \mathbf{x}_m \, \mathrm{d}A \tag{A.1a}$$

$$
\begin{aligned}
&= \frac{1}{V}\bar{\mathbf{F}}_M : \int\limits_{\partial\mathcal{B}_0} (\mathbf{p}_m \otimes \mathbf{X}_m)\,\mathrm{d}A \\
&+ \frac{1}{2\,V}\bar{\boldsymbol{\Gamma}}_M \vdots \int\limits_{\partial\mathcal{B}_0} (\mathbf{p}_m \otimes \mathbf{X}_m \otimes \mathbf{X}_m)\,\mathrm{d}A \\
&+ \frac{1}{6\,V}\,\bar{\overset{4}{\mathbf{E}}}_M :: \int\limits_{\partial\mathcal{B}_0} (\mathbf{p}_m \otimes \mathbf{X}_m \otimes \mathbf{X}_m \otimes \mathbf{X}_m)\,\mathrm{d}A \\
&+ \frac{1}{V}\int\limits_{\partial\mathcal{B}_0} \mathbf{p}_m \cdot \tilde{\mathbf{x}}_m \mathrm{d}A.
\end{aligned}
$$

The first three summands can be identified by comparison of coefficients with eq. (16a) and give the homogenisation rules for the stresses and hyper stresses, cf. eqs. (27a)–(27c). The last summand can be splitted with respect to opposite parts of the microvolume boundary, cf. [23],

$$
\frac{1}{V}\int\limits_{\partial\mathcal{B}_0} \mathbf{p}_m \cdot \tilde{\mathbf{x}}_m \mathrm{d}A = \frac{1}{V}\int\limits_{\partial\mathcal{B}_0^+} \mathbf{p}_m^+ \cdot \tilde{\mathbf{x}}_m^+ \mathrm{d}A + \frac{1}{V}\int\limits_{\partial\mathcal{B}_0^-} \mathbf{p}_m^- \cdot \tilde{\mathbf{x}}_m^- \mathrm{d}A \tag{A.2a}
$$

$$
= \frac{1}{V}\int\limits_{\partial\mathcal{B}_0^+} \mathbf{p}_m^+ \cdot \tilde{\mathbf{x}}_m^+ \mathrm{d}A - \frac{1}{V}\int\limits_{\partial\mathcal{B}_0^+} \mathbf{p}_m^+ \cdot \tilde{\mathbf{x}}_m^+ \mathrm{d}A \tag{A.2b}
$$

$$
= 0. \tag{A.2c}
$$

Opposite parts of the microvolume boundary $\partial\mathcal{B}_0^+$ and $\partial\mathcal{B}_0^-$ are defined such that the identity of the outer normal vectors $\mathbf{N}^- = -\mathbf{N}^+$ holds for corresponding points on $\partial\mathcal{B}_0^+$ and $\partial\mathcal{B}_0^-$. The above-quoted equation (A.2c) is fulfilled for periodic deformations and antiperiodic tractions on opposite parts of the boundary,

$$
\tilde{\mathbf{x}}_m^+ = \tilde{\mathbf{x}}_m^-, \qquad \tilde{\mathbf{p}}_m^+ = -\tilde{\mathbf{p}}_m^-. \tag{A.3a}
$$

* * *

The support by the Deutsche Forschungsgemeinschaft (DFG) is gratefully acknowledged (DI 430/7-1, RA 624/16-1).

REFERENCES

[1] Diebels S. and Steeb H., *Proc. R. Soc. London, Ser. A*, **458** (2002) 2869.
[2] Diebels S. and Steeb H., *Comput. Mat. Science*, **28** (2003) 714.
[3] Diebels S., Johlitz M., Steeb H. and Possart W., *J. Phys.: Conf. Ser.*, **62** (2007) 34.
[4] Tekoğlu C. and Onck P. R., *J. Mech. Phys. Solids*, **12** (2008) 3541.
[5] Capriz G., Podio-Guidugli P. and Williams W., *Meccanica*, **17** (1982) 80.
[6] Cosserat E. and Cosserat F., *Théorie des corps déformables* (A. Hermann et Fils, Paris) 1909.
[7] Eringen A. C., *Polar and Nonlocal Field Theories*, in *Continuum Physics*, Vol. **IV**, edited by Eringen A. C. (Academic Press, New York) 1976, pp. 1-73.

[8] Eringen A. C., *Microcontinuum Field Theories, Vol. I: Foundations and Solids* (Springer, New York) 1999.
[9] Kirchner N. and Steinmann P., *Comput. Mech.*, **40** (2007) 651.
[10] Lazar M. and Maugin G. A., *Philos. Mag.*, **87** (2007) 3853.
[11] Steeb H. and Diebels S., *Proc. Appl. Math. Mech.*, **5** (2005) 319.
[12] Diebels S., Ebinger T. and Steeb H., *J. Mat. Sci.*, **161** (2005) 5919.
[13] Ebinger T., Diebels S. and Steeb H., *Comput. Mech.*, **39** (2007) 815.
[14] Feyel F. and Chaboche J. L., *Comput. Methods Appl. Mech. Eng.*, **183** (2000) 309.
[15] Forest S. and Sab K., *Mech. Res. Commun.*, **25** (1998) 449.
[16] Forest S., *J. Phys. IV*, **8** (1998) 39.
[17] Kouznetsova V. G., *Computational homogenization for the multi-scale analysis of multi-phase material*. PhD-thesis, Technische Universiteit Eindhoven, The Netherlands (2002).
[18] Nemat-Nasser S. and Hori M., *Micromechanics* (North-Holland, Amsterdam) 1993.
[19] Mindlin R. D., *Arch. Ration. Mech. Anal.*, **16** (1964) 51.
[20] Hazanov S., *Arch. Appl. Mech.*, **68** (1998) 385.
[21] Hill R., *J. Mech. Phys. Solids*, **11** (1963) 357.
[22] van der Sluis O., Schreurs P. J. and Brekelmans W. A. M., *Mech. Mat.*, **32** (2000) 449.
[23] Maugin G. A., *The Thermomechanics of Plasticity and Fracture* (CUP, Cambridge) 1992.